Published in final edited form as:

J Biomed Mater Res B Appl Biomater. 2019 August ; 107(6): 1792–1805. doi:10.1002/jbm.b.34272.

Polymeric Ionically Conductive Composite Matrices and Electrical Stimulation Strategies for Nerve Regeneration: *In vitro* Characterization

Ohan S. Manoukian[#1,2], **Scott Stratton**[#1,2], **Michael R. Arul**[2], **Joshua Moskow**[1,2], **Naseem Sardashti**[1], **Xiaojun Yu**[4], **Swetha Rudraiah, PhD**[2,3,*] **[Assistant Professor]**, and **Sangamesh G. Kumbar, PhD**[1,2,*] **[Associate Professor]**

[1]Department of Biomedical Engineering, University of Connecticut, Storrs, CT, USA

[2]Department of Orthopedic Surgery, University of Connecticut Health, Farmington, CT, USA

[3]Department of Pharmaceutical Sciences, University of Saint Joseph, Hartford, CT, USA

[4]Department of Chemistry, Chemical Biology and Biomedical Engineering, Stevens Institute of Technology, Hoboken, USA

[#] These authors contributed equally to this work.

Abstract

Stem cell strategies and the use of electrical stimulation (ES) represent promising new frontiers for peripheral nerve regeneration. Composite matrices were fabricated by coating electrospun polycaprolactone/cellulose acetate micro-nanofibers with chitosan and ionically-conductive (IC) polymers including, sulfonated polyaniline and lignin sulfonate. These composite matrices were characterized for surface morphology, coating uniformity, ionic conductivity, and mechanical strength to explore as scaffold materials for nerve regeneration in conjunction with electrical stimulation. Composite matrices measured conductivity in the range of 0.0049–0.0068 mS/m due to the uniform coating of sulfonated polymers on the micro-nanofibers. Thin films (2D) and composite fiber matrices (3D) of IC polymers seeded with human mesenchymal stem cells (hMSCs) were electrically stimulated at 0.5V, 20Hz for 1h daily for 14 days to study the changes in cell viability, morphology, and expression of the neuronal-like phenotype. *In vitro* ES lead to changes in hMSCs' fibroblast morphology into elongated neurite-like structures with cell bodies for ES-treated and positive control growth factor-treated groups. Immunofluorescent staining revealed the presence of neuronal markers including β3-tubulin, microtubule-associated protein 2, and nestin in response to ES.

Keywords

nerve regeneration; electrical stimulation; ionic conductivity; micro-nanofiber; scaffold

[*]Corresponding Author: Swetha Rudraiah, Department of Pharmaceutical Sciences, School of Pharmacy, University of Saint Joseph, 229 Trumbull Street, Hartford, CT 06103, USA, Office: 860-231-5855, Fax: 860-231-5759, srudraiah@usj.edu, Sangamesh G. Kumbar, Department of Orthopedic Surgery, Department of Biomedical Engineering, Department of Materials Science and Engineering, University of Connecticut, L3096, 263 Farmington Avenue, Farmington, CT 06030-1320, Ph.: 860.679.3955, Fax: 860.679.0347, Kumbar@uchc.edu.

1. INTRODUCTION

Peripheral nerve injury (PNI) is a common injury affecting as many as 1.8% of trauma patients [1] and an estimated 20 million Americans [2], many of whom sustain associated lifelong disabilities. PNI and associated nerve injuries are a significant burden on the health care system resulting in $150 billion USD of medical expenditures annually in the US alone [2]. Despite recent advances in soft tissue surgical techniques, current treatment options involving autografts and allografts suffer from various complications such as donor site morbidity, risk for neuroma, fascicle mismatch, the need for secondary surgeries, and scarring and fibrosis, all of which limit the efficiency and regenerative benefits of this procedure [2, 3].

Despite previous reports predicting nerve regeneration rates of 1–3 mm/day, more recent reports indicate longer than predicted periods [4]. As such, functional recovery does not occur unless the nerve is guided from proximal to distal ends in an efficient manner. Even with aforementioned surgical repair and grafting, these procedures often fail to achieve substantial functional recovery, particularly if the injury spans longer distances. Such injuries can take months and upwards of years to regenerate, often with suboptimal results [5]. Alternatives to current surgical treatments present a critical unmet need, and techniques focusing on tissue engineering and stem cell approaches are promising [6–9].

Cell therapies, including Schwann cells, induced pluripotent stem cells, and neuronal stem cells, are an attractive therapeutic option for treating PNI, and have been explored with limited success, particularly limited by their lack of feasible clinical translation. As such, significant attention has been turned to the transplantation of human mesenchymal stem cells (MSCs) for PNI and nerve regeneration due to their clinical feasibility and relative ease of harvesting, culturing, and integration. Recent studies suggest that MSCs can show unorthodox plasticity, transdifferentiating into non-mesoderm lineages, including neuronal phenotypes via chemical growth factor treatments [10–14]. The use of growth factors, such as brain derived neurotrophic factor (BDNF), nerve growth factor (NGF), and basic fibroblast growth factor (bFGF), have been documented extensively to demonstrate MSC differentiation and nerve regeneration [10–12, 15]. Despite encouraging results, growth factor strategies often induce complicated, complex chemical and biological interactions which may result in unpredictable, adverse effects, limiting their feasibility in clinical use [16, 17]. As such, alternate means of potential MSC differentiation for nerve regeneration applications may prove significantly beneficial to elucidate pathways responsible for trans-differentiation and correlated nerve regeneration.

The benefits of electrical stimulation (ES) in the regeneration of bone, cartilage, skin, spinal nerves, and most relevantly, peripheral nerves have been widely discussed and demonstrated in literature [4, 18–22]. ES has been widely used in physical therapy to improve functional recovery of muscle and nerve tissue injuries and has been shown to enhance tissue regeneration [23, 24], most often using electrically-conducting polymers as scaffolds, including polyaniline (PANI), polypyrrole, polyacetylene, and poly(3,4-ethylenedioxythiophene) [25, 26]. Although the advantages of using ES in conjunction with such polymers have been shown for enhancing nerve outgrowth, extension, and regeneration

[21], electrically-conducting polymers are limited in performance as they rely on electrons and holes for conduction and are known to deteriorate in physiologic environments due to redox instability, significantly affecting their long-term conductivity. Furthermore electrically-conducting polymers have other limitations including processing challenges, brittleness, hydrophobicity, non-degradability [25–27].

Ionically conductive (IC) biomaterials represent a new generation of smart materials used for electrical stimulation and recording [28, 29]. IC biomaterials can be used to deliver cells, bioactive factors, and facilitate ES at the site of implantation to promote tissue regeneration [30]. These biodegradable materials disintegrate and are removed from the body after completion of their functions [31]. Biopolymers such as chitosan [32], agarose [33], β-cyclodextrin [34], cellulose [35], starch [36], alginate [37] and hyaluronic acid [38] have been used for tissue engineering applications [39, 40]. Introducing ionizable groups on the polymer backbone enables polymers to conduct electricity in a physiological environment through counter flow of ions when electrical potential is applied [41, 42]. These IC polymers exhibit a conductivity dependent on the number of ionizable groups on the polymer backbone, and not on the number of available electrons and holes for charge movement [43, 44]. This represents a conducting mechanism that is fundamentally different from aforementioned, commonly used, electrically-conducting polymers which have been previously reported for nerve regeneration applications (Figure 1) [41, 45, 46].

Previously, we have reported the synthesis and characterization of ionically conductive sulfonated polymers and evaluated their potential for tissue engineering applications [41]. Various formulations of sulfonated conductive polymers were shown to have differing water contact angles and electrical conductivities, where the conductivity was shown to be directly proportional to the sulfonic content. Furthermore, these sulfonated polymers demonstrated superior cell adhesion properties, compared to cells seeded onto tissue culture polystyrene, and supported proliferation of human skin fibroblasts over 14 days [41]. As such, ionic materials formulated using sulfonated polymers have tremendous appeal as scaffolds for various tissue engineering and regenerative medicine applications [41].

Electrospun nanofiber matrixes closely mimic the native extracellular matrix (ECM) components and have been explored for a variety of tissue engineering applications [47–51]. Electrospun polycaprolactone (PCL) micro-nanofibers, and their composites, are well-suited for tissue engineering applications, due to their ease of processability, biocompatibility, and long-term biodegradability. PCL is often blended with other hydrophilic polymers, including poly(ethylene glycol) (PEG) and cellulose acetate (CA) to promote cell adhesion and promote matrix degradation/erosion[51–54]. Chitosan (CHT) a polysaccharide carries a positive charge in its hydrated form and extensively used as a scaffolding material for tissue engineering and drug delivery applications [55, 56].

In the present study, we first investigated the effects of ES on the morphology and phenotypic development of human mesenchymal stem cells toward neuronal-like cells. These preliminary 2-dimensional (2D) studies were conducted on glass coverslips coated with CHT with sulfonated polyaniline (SPANI) followed by cross-linking, which allowed for the ability to utilize phase-contrast microscopy as well as typical staining techniques (Figure

2). Subsequently we investigated the effects of 3-dimentional (3D) ionically conducting polymers in conjunction with ES. PCL-CA micro-nanofiber matrices were coated with CHT and blends of CHT with SPANI and CHT with lignin sulfonate (LS) to modify scaffold physicochemical properties including ionic conductivity, erosion rate, and strength. These matrices were evaluated for *in vitro* human mesenchymal stem cells attachment, viability, changes in morphology, and neuron-like phenotype development under the influence of electrical stimulation.

2. EXPERIMENTAL

2.1 Materials

Polycaprolactone (MW 80,000), cellulose acetate (MW 30,000), chitosan (medium molecular weight), lignin sulfonate (MW 8,000), aniline, and propane sultone were purchased from Sigma Aldrich (Saint Louis, MO). Circular glass cover slips, potassium persulfate, acetone, and methylene chloride were purchased from Fisher Scientific (Fair Lawn, NJ). Phosphate buffered saline (PBS, Cat# 10010–023) from Gibco (Grand Island, NY), and ethanol was purchased from Brand Nu Lab (Meriden, CT). LIVE/DEAD™ Viability/Cytotoxicity Kit was purchased from Life Technologies (Cat# L3224 Life Technologies, Eugene, Oregon) and Quant-iT™ PicoGreen™ dsDNA Assay Kit (Cat# P7589) were purchased from Thermo Fisher Scientific (Waltham, MA). For all cell studies, human MSCs (Cat# PT-2501) and Dulbecco's Modified Eagles Medium (DMEM, Cat# 12–604F) were purchased from Lonza (Walkersville, MD). Fetal bovine serum (FBS, Cat# 10437028) and penicillin/streptomycin (P/S, Cat#15140122) were purchased from Gibco (Grand Island, NY). All primary and secondary antibodies were purchased from Abcam (Cambridge, MA). Voltage maps, field modeling, and FEA analyses were done using the QuickField DC conduction module (Tera Analysis Ltd., Svendborg, Denmark). All reagents and solvents were used without further purification. Millipore water was used for every experiment using the Milli–Q plus system (Millipore Sigma Burlington, MA).

2.2 Preparation of Sulfonated polyaniline (SPANI)

Sulfonated polyaniline (SPANI) was prepared by polymerization of sulfonated aniline according to the published literature [57]. In brief, 5 mL of aniline and 1.35 g of propane sultone in acetone were allowed to stir at room temperature for 6 h to obtain sulfonated aniline monomer. The monomer was filtered and washed with acetone to remove unreacted reagents and dried under vacuum. Potassium persulfate was added at a 1:1 ratio with the monomer in 50% aqueous ethanol was stirred overnight at room temperature to obtain SPANI. Final product was obtained by filtration and dialyzed using cellulose dialysis membrane (MW cutoff 3,000 Da) for 24 h. The purified product was obtained by lyophilization overnight. The structure of the synthesized polymer was confirmed by spectroscopy.

2.3 *In vitro* cell studies on SPANI-coated 2D glass

Preliminary studies investigated hMSCs morphology, viability, and phenotypic development on a 2-dimensional (2D) glass coverslips coated with CHT+SPANI and cross-linked with epichlorohydrin [19]. Cell morphology was analyzed using light (phase-contrast)

microscopy, while cell viability and phenotype expression utilized LIVE/DEAD™ and immunofluorescent staining, respectively. Each cover slip (11 mm diameter) was sterilized in aqueous 70% ethanol for 20 minutes, followed by exposure to UV light for 35 minutes. Glass coverslips were placed in 24-well tissue culture plates and incubated in basal media at 37°C overnight prior to seeding cells.

After overnight incubation, 10,000 cells were seeded and allowed to adhere for 4 hours, prior to the addition of remaining media consisting of DMEM supplemented with 10% FBS and 1% P/S. Cells were treated with ES at 0.5V, 20Hz for 1 hour daily up to 14 days and compared to untreated controls. For cell morphology studies, NGF was added at a concentration of 50 ng/mL [58], serving as the positive control. The custom-built electrical stimulation plate and the in vitro stimulation set up is shown in Figure 3. In this set up a positively charged gold ring touches the outer edges of the sample with a ground ring touching the center, such that current travels from the outer edges toward the center in response to a voltage difference.

2.4 Preparation of PCL/CA micro-nanofibers

Fiber matrices comprised of micro-nanofibers were fabricated using electrospinning technique as per our previous work with few modifications [59]. Polycaprolactone and cellulose acetate in the ratio of 80:20 were dissolved in an admixture of methylene chloride and ethanol (85:15 ratio) to obtain a final polymer concertation of 12% (w/v). This polymer solution was electrospun onto a rotating target using the electrospinning parameters of 2.5 mL/h flow rate, 18G needle, 20 cm working distance, 15kV applied voltage and ambient conditions of temperature/humidity [60].

2.5 Preparation of 3D composite micro-nanofibers

Fiber lattices were coated with ionically conductive water soluble polymers to obtain composite fiber matrices per our published work with few modifications [61]. A 3 wt. % chitosan solution in 2% aqueous acetic acid was used to apply the coating on the fiber lattice. In brief, fiber lattice was incubated in the chitosan solution to allow infusion under vacuum in a plastic bag. Solution infused fiber lattice was immersed in alkaline epichlorohydrin solution (0.01 mol/L) prepared in NaOH solution (0.067 mol/L) at 40 °C for 2 hours [19]. After this period, the membranes were rinsed with deionized water to remove the unreacted epichlorohydrin [62, 63]. Cross-linked composite matrices were washed repeatedly with DI water to remove unreacted epichlorohydrin and allowed to dry in air and kept desiccated until further use. Similarly, 20 wt. % of lignin sulfonate or SPANI was mixed with 3 wt. % was mixed with chitosan as explained above and applied to fiber lattice coating followed by cross-linking. The control micro-nanofiber lattice was coded as PCL/CA and other test groups with chitosan, lignin sulfonate and SPANI were PCL/CA +CHT, PCL/CA+CHT/LS and PCL/CA+CHT/SPANI respectively.

2.6 Fourier transform infrared spectroscopy (FTIR)

Fourier transform-infrared spectroscopy was used to confirm presence of ionic groups on the fiber matrices at various stages of its incubation in cell culture media. Dry composite matrix

samples were used to acquire a total of 32 scans in the wavelength range of 4000cm^{-1} to 500cm^{-1}and processed using Thermo Scientific Smart FTIR technology.

2.7 Scanning electron microscopy (SEM)

Scanning electron microscopy was used to examine the surface morphology of composite matrices. Samples were sputter coated with gold using Hummer V sputtering system (Technics Inc., Baltimore, MD) and imaged using JEOL 6335F FESEM (Boston, MA, USA) technology at 20kV operating voltage and 1000X magnification. Composite matrices of each type (n=3) were imaged at three different locations and representative images are presented in the manuscript.

2.8 Weight loss measurements

Conductivity of composite matrix is dependent on the presence of chitosan and ionic polymer derivatives such as lignin sulfonate and SPANI at various stages of cell culture experiments. Therefore, matrix weight loss studies were performed in phosphate buffer pH 7.4 at 37 °C over a period of 25 days. Every other day incubation media PBS was changed every other day in order to maintain a consistent concentration gradient and *in vivo* cell culture condition. Equal weight of control fiber matrices and composite matrices (test groups) in triplicate were incubated in PBS in 6-well plates. These samples were allowed to equilibrate overnight and the equilibrium weight was measured with a Mettler Toledo XP56 DeltaRange balance with a sensitivity of 0.002 mg (Mettler Toledo, Columbus, OH). The initial equilibrium weight for all the matrices was presented as 100% and relative weight loss over a period of 25 days is presented as a percent weight loss [64]. Measurements are presented as mean ± standard deviation of n=3 for each type and each timepoint.

2.8 Mechanical testing

Fiber control lattice and composite matrices were subjected for mechanical properties in tensile mode an Instron 5544 Universal Testing system (Instron, Norwood MA). Dog bone shaped samples measuring 20×10 mm (length/breadth) were hydrated overnight in PBS at 37°C prior to testing per the ASTM guidelines [65]. Samples were pulled at a rate of 10 mm/min until failure to obtain the stress-strain curve. Tensile strength and Young's modulus were calculated and presented as mean ± standard deviation of 6 samples.

2.9 Conductivity analysis

For conductivity measurements, 2-inch^2 samples were used in a two-point contact clamping system to obtain electrical resistance using an ohmmeter (Keithley Integra Series 2700) [66]. Samples in triplicate (n=3) were utilized for these measurements. In brief, the selected sample was fixed to the instrument base and clamped on both sides, as resistance is observed until a constant value is obtained. Electrical conductivity α is calculated using Equation 1, where L is sample thickness, R is resistance from the two-point contact system, A is surface area of the sample.

$$\alpha = \frac{L}{RA} \quad (1)$$

2.10 Thermogravimetric analysis (TGA)

Control and composite test group samples were subjected for TGA analysis using TGA Q-500 (TA Instruments, New Castle, DE) to measure the amount of coating retained. In brief, ~10 mg samples dry samples in a platinum TGA trays were heated from 10–800°C with an equilibrium temperature of 200°C under nitrogen purging. Universal Analysis software associated with the instrument was used to obtain thermograms corresponding to weight loss as a function of temperature.

2.11 Human Mesenchymal Stem Cells (hMSCs)

Control and composite fiber matrices were cut into circular discs measuring 11 mm in diameter and immersed in aqueous 70% ethanol for 20 minutes, followed by exposure to UV light for 35 minutes on each side for sterilization. Scaffold discs were placed in non-treated tissue culture 24 well plates and incubated in basal media at 37°C overnight prior to seeding cells.

Each scaffold was seed with 50,000 cells (passage #5) in 50μL cell suspension and allowed to attach on the scaffold for 4 hours prior to adding media. Post-adhesion, 1mL of basal media was added for control and ES treatment groups, while positive control groups received media supplemented with 50 ng/mL[58] of NGF. Media was changed every other day for all the groups and ES was applied every day at 0.5V, 20Hz for 1 hour daily using the aforementioned custom-built cell stimulation system. Cell culture experiments were carried out for a period of 14 days and biological samples were harvested at various time points of to study cell attachment, viability, morphological changes, and neuronal-like phenotype expression via immunohistochemistry. For all measurements a sample size of n=3 for each time point and treatment group was used.

2.12 Cell viability

Cell viability under various treatment groups was accessed using a fluorescence-based LIVE/DEAD™ cell viability assay according to the manufacturer's instructions. At specific timepoints isolated biological samples were washed with warm PBS and incubated with ethidium bromide and calcein [67]. Ethidium bromide penetrates the membranes of dead cells and red excitation occurs upon binding to nucleic acids. Calcein excites green upon binding to esterase in the intracellular environment. Samples were imaged at various magnifications using a confocal microscope (Zeiss LSM 880) at different spots of the scaffold. For all measurements a sample size of n=3 for each time point and treatment group was used.

2.13 Immunofluorescent staining

Immunofluorescent staining was performed in order to examine the presence of neuronal-specific proteins in ES-treated groups, compared to non-treated groups. Briefly, samples

were washed using PBS (all washes performed in triplicate) to get rid of cell culture medium and were fixed for 30 minutes using 4% paraformaldehyde (Sigma, St. Louis, MO) in PBS solution followed by rinsing with PBS. Samples were permeabilized using 0.2% Triton X-100 prepared in PBS for 10 minutes then washed with PBS. Proteins were blocked by incubating with 1% bovine serum albumin (BSA) in PBST (PBS with 0.1% Tween 20) for 30 minutes at room temperature followed by PBS wash. The primary neuronal antibodies, anti-NSE (ab53025, 1:100), anti-GFAP (ab7260, 1:1000), anti-mouse β-III Tubulin (ab18207, 1:1000), anti-rabbit MAP2 (ab32454, 1:200), and anti-nestin (ab22035, 1:100) were all diluted to their respective ratios in 1% BSA in PBST, and 150μL of solution was placed on respective samples. Samples were incubated with primary antibody solution overnight at 4°C. The following day samples were washed 3 times with PBS followed by incubation for 1 hour with secondary antibodies, Rhodamine Red (goat anti-rabbit, ab6719) and Alexa Flour 488 (goat anti-mouse) (ab150113, Abcam, Cambridge, MA), in 1:200 ratios and carefully protected from light. Lastly, samples were PBS washed prior to viewing via confocal microscopy. For all these measurements a sample size of n=3 for each time point and treatment group was used.

2.14 Statistical analysis

All data is expressed as mean ± standard deviation. All results were first evaluated using one-way analysis of variation (ANOVA) followed by Dunnett's multiple comparisons test with a confidence of 95% using GraphPad Prism 7 (GraphPad Software, Inc. La Jolla, CA).

3. RESULTS

3.1 2D Electrical Stimulation and Cell Differentiation

Preliminary studies looked at the influence of electrical stimulation on hMSCs seeded on to glass cover slips coated with epichlorohydrin cross-linked CHT/SPANI in terms of their morphology, viability, phenotypical changes towards neuronal lineages *in vitro* over a period of 14 days. A custom-built electrical stimulation system was designed in house for these experiments (Figure 3A). The system was designed to deliver equal voltage to each well, when used in conjunction with a standard 6-well plate, and was validated and verified by voltmeter testing and FEA conductivity modeling (Figure 3B) [68]. Modeling was achieved by designing and simulating 13.25mm mesh with a single negative node in the center, set to a defined voltage of −3V, and an outer ring set to with an arbitrary 3V. To more accurately mimic the intended use, the model was set in an ideal conducting medium having a conductivity of 200 mS/cm. The voltage distribution was calculated and mapped to have a predictably linear decrease from the outer ring toward the inner ground. An inflection can be seen where the voltage (and subsequently the current, data not shown) decreases at a quicker rate, potentially corresponding to the 3-dimensional draw towards the center ground node from the media.

Cells were observed to have changed morphologies under the influence of ES, more closely resembling the positive control NGF-treatment, while maintaining typical fibroblast hMSC morphology in untreated control (Figure 4A). The morphology of ES-treated hMSCs qualitatively resembles positive control (PC) samples treated with NGF, which show long

axon-like branches with a cell body, characteristic of neuronal cells. Morphological changes exhibited by ES-treated cells were further analyzed by quantification of dimensionality. Measurements of cytoskeletal protrusion length and breadth at day 10 show statistically significant differences between untreated negative controls and ES-treated groups (Figure 4B). Untreated cells showed a mean length of 301.8±52.54 μm, while NGF- and ES-treated cells measured 446.0±81.37 and 438.4±70.93 μm, respectively. Similarly, untreated cells showed larger mean cell width/breadth, measuring 53.85±14.92 μm, while NGF- and ES-treated cells measured 13.33±9.08 and17.59±17.43 μm, respectively. Image analysis was conducted using ImageJ (NIH, Bethesda, MD) where each measurement on the graph is taken at three different spots on the same sample including at least 100 cells and presented as an average. The effects of ES on cell viability and proliferation were analyzed qualitatively using dual-color, live/dead fluorescence staining. At all three timepoints, up to and including day 10, cells treated with ES showed no noticeable differences in their viability and proliferation as compared to untreated control cells (Figure 5).

Figure 6 summarizes immunofluorescent staining for early and late neuronal markers to elucidate potential cell differentiation into neuronal lineages. Early protein markers, including Glial fibrillary acidic protein (GFAP) and Neuron Specific Enolase (NSE), were expressed at all the time points of 3, 7, and 14 days. Untreated controls (Figure 6A-C) showed minimal expression of GFAP (stained green), but did not show prominent expression of NSE (stained red). In contrast, ES-treated cells (Figure 6D-F) showed substantial expression of both GFAP and NSE at all timepoints.

Late (mature) protein markers including Microtubule-Associated Protein 2 (MAP2)and Beta-III Tubulin (B3TUB), expressions were low on Day 3, as expected, and increased with culture time [72, 73]. Untreated controls show staining for B3TUB (stained green), but no substantial staining for MAP2 (stained red) (Figure 6G-I). ES-treated cells show substantial B3TUB and MAP2, particularly at later timepoints day 7 and day 14 (Figure 6J-L).

3.2 3D Composite Matrix Scaffold Characterization

3.2.1 Scanning electron microscopy (SEM)—

The macro-structure of fiber lattice and their composite matrices coated with ionically conductive polymers as tissue engineering scaffolds is shown in Figure 7. The fiber lattice is comprised of micro-nanofibers with diameters in the range of 1.5±300μm for microfibers and nanofibers in the range of 250–900 μm. Composite matrices are covered uniformly with ionically conductive polymer derivatives. No significant differences were observed in morphology between the groups coated with LS and SPANI.

3.2.2 Conductivity analysis—

The variation in matrix conductivity following incubation in PBS at 37ºC over a period of 28 days is summarized in Figure 8A. Fiber matrices showed uniform sulfonated polymer coating and conductivity was in the range of 0.0049–0.0068 mS/m based on the matrix composition. Conductivity of the matrices decreased with matrix erosion and at any given time conductivity was higher than the neat chitosan coated matrix, up to 28 days *in vitro.* Fiber matrix conductivity increases in the order of PCL/CA, PCL/CA+CHT, CHT/LS, and CHT/SPANI at all timepoints. The varying

degrees of conductivity are dependent on the ion exchange capacity (IEC) and density of ionic groups on the composite matrices. Specifically, the high conductivity of PCL/CA +CHT/SPANI is due to the conjugation of pi-bonds when the benzene ring is attached to the sulfonic group.

3.2.3 Fourier transform infrared spectroscopy (FTIR)—Chemical structure and interactions of fiber lattice and coated composite fiber matrices was determined using FTIR (Figure 8B). The fiber lattice confirms the presence of PCL and CA through the characteristic ester peak at 1724 cm^{-1} [75] and methyl group at 1370 cm^{-1}, respectively [76]. While composite fiber matrices coated with chitosan shows the presence of amine groups at 1650 cm^{-1} [77], and -OH and -NH bonds between 3357 cm^{-1} and 3284 cm^{-1} respectively [78]. LS- and SPANI-coated composite matrices showed additional aromatic sulfonated groups at 1070 cm^{-1} [79]. These results confirm the presence of ionically conductive polymers presence on PCL-CA fiber lattice.

3.2.4 Weight loss/polymer leaching—Tissue engineering scaffolds and biomatrices should allow proper tissue infiltration over time as they degrade following implantation. In the present study, scaffolds were evaluated for their percent weight loss due to the erosion of the coated matrix on the fiber lattice. The rate of polymer erosion has residual effects on matrix tensile properties and ionic conductivity. As the polymer undergoes erosion or degradation, mechanical properties tend to decrease, owing to a lack of material. Similarly, as the ionically-conducting coating erodes away, there is to be an expected drop in conductance, however minor. Figure 8C summarizes the percent weight loss profile for all the matrices over a period of 25 days in PBS incubated at 37ºC. The weight loss trend decreased in the order of PCL/CA+CHT/SPANI, PCL/CA+CHT/LS, PCL/CA+CHT, and PCL/CA. Highly water soluble ionic derivatives namely LS and SPANI leach out from the composite matrices over time accounting for the matrix weight loss. As such, both LS- and SPANI-coated scaffolds show substantial weight loss at the end of 25 days, as compared to the other groups. However, due to their hydrophilic nature, oftentimes water absorption can be seen, resulting in minor increases in weight and upward inflections which can be seen in the weight loss chart, resembling a pulsatile pattern. As a result, these matrices show a decreasing trend in conductivity eventually leveling to that of PCL/CA+CHT following the end of the study.

3.2.5 Thermogravimetric analysis (TGA)—TGA was performed on all matrices to investigate the thermal stabilities of composite matrices at day 1 and 28. TGA is a technique where the mass of a polymer or material is measured as a function of temperature or time while the sample is subjected to a controlled temperature regime [80]. The thermograms presenting weight loss patterns are presented in Figure 8D. Mass loss if often categorized as volatile compounds (residual moisture and solvents) generally evaporate between ambient and 300 °C, while degradation of products resulting from chain scission often require temperatures above 200 °C [80]. The thermal weight loss for polymer matrices was shown to be tri-phasic for all matrices approximately at ~120 °C (water), ~390 °C (functional groups), and ~523 °C (polymer backbone). The identical weight loss patterns for both the samples collected at two timepoints confirm the presence of coating material, if not on the surface

but within the fiber lattice, and contribute to the aforementioned conductivity and weigh loss characteristics.

3.2.6 Mechanical properties—Fiber lattice and composite matrices were evaluated for their tensile properties in the hydrated state following 24 h soaking in PBS (pH 7.4). Figure 9A/B graphically depicts the Young's modulus and tensile strength, respectively. The increased modulus observed with composite matrices is attributed to the brittle nature due to the presence of another polymer phase as a coating. The elastic nature of fiber-based matrix lattice resulted in higher tensile strength as compared to composite matrices due to the presence of the hydrogel-like coating in the solvated state.

3.3 3D Scaffold Electrical Stimulation and Cell Differentiation

Cell morphology and viability on 3D composite fiber matrices was investigated using live/dead staining (Figure 10). Viable cells were found for all polymer composite derivatives and for all treatment groups, namely untreated control, NGF-treated positive control, and ES-treated cells. These images also reflect similar observations to those of 2D culture experiments where hMSCs were seeded on glass coverslips coated with ionically conducting polymers (Figure 5). Furthermore, in a preliminary immunofluorescence study, hMSCs treated with ES show positive staining for three prominent neuronal protein markers: B3TUB, MAP-2, and Nestin (Figure 11). The pilot study showed electrically stimulated hMSCs expressed B3TUB, a protein marker for neuronal differentiation responsible for axon guidance, maintenance and neurite extension, MAP-2, a protein responsible for neurogenesis and dendrite structure, and Nestin, an intermediate filament protein required for survival, renewal, and proliferation of neuronal cells.

4. DISCUSSION

The formulations of degradable micro-nanofiber PCL/CA scaffolds coated with ionically-conductive polymers LS and SPANI represent novel biomaterial-based methods for overcoming the common limitations of electrically-conductive polymers. Ionically-conducting membranes allow for polymers to conduct electricity in a physiological environment through counter flow of ions when electrical potential is applied. This conduction mechanism is only dependent on the number of ionizable groups on the polymer backbone, and not on the number of available electrons and holes for charge movement, making it highly novel, advantageous, and desirable for biomedical and physiological applications including tissue engineering and regenerative medicine.

The combination of micro- and nanofibers allows for control of appropriate porosity, allowing for cell penetration, and adequate nutrient and factor transport, whilst also granting superior cell adhesion and mechanical properties. In order to facilitate peripheral nerve regeneration, scaffold properties must accurately mimic the intrinsic properties of the native nerve tissues. Nerve tissue, being highly vascularized, demands a highly porous scaffold capable of adequate cell penetration and adhesion in order to enable the infiltration and development of the nerve axons and blood vasculature within and/or through the scaffold network. The micro-nano features of the studied scaffold allow for tunable pore properties, whereas solely micro-, or solely nano-, structures would result in too little and too much

porosity, respectively. Furthermore, the combination of micro-nanofibers grants adequate mechanical properties, critical for successful integration of the scaffold, aiding in its regenerative capabilities. In contrast, nanofibers alone suffer from a lack of mechanical integrity, a common limitation of polymeric nanomaterials.

Mechanical properties of tested scaffolds showed changes in modulus and tensile strength dependent on the differing degrees of hydration, corresponding to the multi-material composite matrices. These results are consistent with earlier reports in literature suggesting decreased strength in multi-phased composite materials [81]. The presence of LS and SPANI in composite matrices, due to their acidic nature, can promote hydration of chitosan subsequently resulting in weaker strength composites. Hydrogels in general have been reported to possess lower tensile strengths due to water content and cross-linked networks [82]. However, the composite matrices offer tensile properties superior to hydrogel-only scaffolds and retain much required mechanical properties desirable for soft tissue and nerve regeneration. Similarly, there were detectable differences in ionic conductance between formulation, with the varying degrees of conductivity dependent on the ion exchange capacity (IEC) and density of ionic groups on the composite matrices. Specifically, PCL/CA +CHT/SPANI showed high conductivity, due to the conjugation of pi-bonds when the benzene ring is attached to the sulfonic group.

Human mesenchymal stem cells treated with electrical stimulation show a clear and distinct morphological deviation from those of untreated, negative control groups, where treated cells show extension, branched and networked structures, while negative control samples display typical fibroblastic, spindle-shaped morphology [69]. Cells treated with NGF (positive control) and ES (treatment group) showed elongated cell morphology and dendritic-like morphological changes, which have been well documented in stem cells in the process of differentiating structures resembling neuron like cells [83–85]. These findings also suggest cell viability and morphological changes in 3D environment under the influence of ES [86–88]. Similar to our previous ES studies, conducted on 2D glass coated with ionically-conducting SPANI, cells treated with ES on 3D fiber composite matrices showed qualitative changes in morphology. Increase in cell length and protrusion was very prominent in ES- and NGF-treated (positive control) groups, but not in untreated (negative control) groups ($p<0.05$). The increase in cell length, in combination with cell width/breadth decrease, is also indicative of neuron-like morphology.

Positive immunofluorescence stains for both early (GFAP and NSE) and mature (B3TUB and MAP2) neurogenic markers and morphological changes also support potential ES-mediated hMSC differentiation into neuronal lineage on ionically conductive polymer. Glial fibrillary acidic protein (GFAP) is an intermediate filament (IF) III protein found in central nervous system and the peripheral nervous system, where enteric Schwann cells and satellite cells of human sensory ganglia express GFAP [70] . Neuron Specific Enolase (NSE) is a neurotrophic and neuroprotective protein often associated with cell survival [71]. Beta-III Tubulin (B3TUB) is a major protein constituent of microtubules and plays a critical role in proper axon guidance and maintenance [74]. Microtubule-Associated Protein 2 (MAP2) is a neuron-specific protein that promotes assembly and stability of the microtubule network [72].

The expression of neuronal markers and morphological changes of hMSCs cultured and treated on 3D ionically conducting micro-nanofiber scaffolds compliment the findings of the aforementioned studies on 2D coated glass. These findings are in agreement with the differentiation of hMSCs by other groups *via* various of chemical means, as reported in literature, and strongly suggest that hMSCs are capable of transdifferentiating into neuronal-like lineages when treated with electrical stimulation *in vitro* [10–12, 15]. However, further studies are needed to elucidate cellular mechanisms and dictate definitive transdifferentiation. Ongoing studies are underway which further characterize differentiating hMSCs, including gene, RNA, and protein expression analyses, as well as functional assessments of differentiated cells. Utilizing ionically conductive polymers, in conjunction with ES, may help differentiate hMSCs into neuronal or Schwann cell-like lineages and proper biocompatibility and adhesion can be sufficient for macrophage and Schwann cell recruitment, nutrient transportation, and ultimately bands of Büngner formation for enhanced healing, repair, and regeneration of peripheral nerves.

5. CONCLUSIONS

Electrical stimulation showed profound effects on hMSC morphology and protein expression when treated on 2D glass coated with ionically conductive sulfonated polyaniline. Cells treated with ES showed significantly different dimensionality, with longer protrusions and decreased breadth, resembling positive control groups, when compared to untreated cells. Cellular attachment and viability on was unharmed with ES, and ES-treated cells showed positive expression of GFAP, NSE, B3TUB, and MAP2 over a 14-day study. In an effort to develop tissue engineering scaffolds to facilitate ES for nerve regeneration, micro-nanofiber scaffolds of PCL/CA and their ionically conductive derivatives were prepared using chitosan, sulfonated polyaniline, and lignin sulfonate. The SEM images of fabricated composite fibers demonstrated an interconnected porous structure with randomly orientated fibers and a conductive hydrogel layer. The polymeric composites stabilized after a two-week period in physiological conditions, retaining most of their conductivity. Following incubation in physiological conditions, tensile properties revealed brittle nature in hydrogel groups and an elastic nature in the PCL/CA nanofiber group. The presence of SPANI and LS led to decreased tensile strength due to the hydrophilicity of the materials allowing for greater aqueous infiltration and thus pre-stretching of fibers. *In vitro*, ES with ionically conductive 3D polymer matrices showed a profound effect on the morphology of hMSCs as compared to non-treated groups, where ES-treated cells showed neurite-like extension and dendritic-like structures, similar to those findings of studies on 2D coated glass. Immunofluorescent staining for B3TUB, MAP2, and Nestin neuronal protein markers revealed qualitatively dense concentrations of all three proteins at 14 days. As such, the development and testing of ionically-conductive polymer scaffolds, in conjunction with electrical stimulation, has strong potential for peripheral nerve regeneration applications and may help differentiate human Mesenchymal stem cells into neuronal or Schwann cell-like lineages. The proper biocompatibility, mechanical properties, cell adhesion and infiltration may be vital in facilitating Schwann cell recruitment, growth factor dispersion and transport, and ultimately axonal outgrowth for nerve regeneration applications.

ACKNOWLEDGEMENTS

The authors acknowledge funding support from the National Institute of Biomedical Imaging and Bioengineering of the National Institutes of Health (R01EB020640), and the Connecticut Regenerative Medicine Research Fund (15-RMBUCHC-08), the Department of Defense (OR120140) and National Science Foundation (NSF) (EFRI-1332329). Ohan S. Manoukian is the recipient of the NSF Graduate Research Fellowship (Grant No. DGE-1747453). Authors also acknowledge the contributions of Rita Matta, Justin Letendre, and Paige Collins for the design and preliminary testing of the electrical stimulation plate.

References

[1]. Taylor CA, Braza D, Rice JB, and Dillingham T, “The incidence of peripheral nerve injury in extremity trauma,” American Journal of Physical Medicine & Rehabilitation, vol. 87, pp. 381–385, 2008. [PubMed: 18334923]

[2]. Grinsell D and Keating C, “Peripheral nerve reconstruction after injury: A review of clinical and experimental therapies,” BioMed research international, vol. 2014, 2014.

[3]. Anderson M, Shelke NB, Manoukian OS, Yu X, McCullough LD, and Kumbar SG, “Peripheral nerve regeneration strategies: electrically stimulating polymer based nerve growth conduits,” Critical Reviews™ in Biomedical Engineering, vol. 43, 2015.

[4]. Al-Majed AA, Neumann CM, Brushart TM, and Gordon T, “Brief electrical stimulation promotes the speed and accuracy of motor axonal regeneration,” Journal of Neuroscience, vol. 20, pp. 2602–2608, 2000. [PubMed: 10729340]

[5]. Kline DG and Hudson AR, Nerve injuries: operative results for major nerve injuries, entrapments, and tumors: Saunders, 1995.

[6]. Manoukian O, Ahmad A, Marin C, James R, Mazzocca A, and Kumbar S, “Bioactive nanofiber dressings for wound healing,” Wound Healing Biomaterials-Volume 2: Functional Biomaterials, p. 451, 2016.

[7]. Lee P, Manoukian OS, Zhou G, Wang Y, Chang W, Yu X, et al., “Osteochondral scaffold combined with aligned nanofibrous scaffolds for cartilage regeneration,” RSC Advances, vol. 6, pp. 72246–72255, 2016.

[8]. Stratton S, Manoukian OS, Patel R, Wentworth A, Rudraiah S, and Kumbar SG, “Polymeric 3D printed structures for soft-tissue engineering,” Journal of Applied Polymer Science, 2017.

[9]. Manoukian OS, Matta R, Letendre J, Collins P, Mazzocca AD, and Kumbar SG, “Electrospun Nanofiber Scaffolds and Their Hydrogel Composites for the Engineering and Regeneration of Soft Tissues,” Biomedical Nanotechnology: Methods and Protocols, pp. 261–278, 2017.

[10]. Keilhoff G, Goihl A, Langnäse K, Fansa H, and Wolf G, “Transdifferentiation of mesenchymal stem cells into Schwann cell-like myelinating cells,” European journal of cell biology, vol. 85, pp. 11–24, 2006. [PubMed: 16373171]

[11]. Kingham PJ, Kalbermatten DF, Mahay D, Armstrong SJ, Wiberg M, and Terenghi G, “Adipose-derived stem cells differentiate into a Schwann cell phenotype and promote neurite outgrowth in vitro,” Experimental neurology, vol. 207, pp. 267–274, 2007. [PubMed: 17761164]

[12]. Caddick J, Kingham PJ, Gardiner NJ, Wiberg M, and Terenghi G, “Phenotypic and functional characteristics of mesenchymal stem cells differentiated along a Schwann cell lineage,” Glia, vol. 54, pp. 840–849, 2006. [PubMed: 16977603]

[13]. Brohlin M, Mahay D, Novikov LN, Terenghi G, Wiberg M, Shawcross SG, et al., “Characterisation of human mesenchymal stem cells following differentiation into Schwann cell-like cells,” Neuroscience research, vol. 64, pp. 41–49, 2009. [PubMed: 19428682]

[14]. Mahay D, Terenghi G, and Shawcross SG, “Schwann cell mediated trophic effects by differentiated mesenchymal stem cells,” Experimental cell research, vol. 314, pp. 2692–2701, 2008. [PubMed: 18586239]

[15]. Tohill M, Mantovani C, Wiberg M, and Terenghi G, “Rat bone marrow mesenchymal stem cells express glial markers and stimulate nerve regeneration,” Neuroscience letters, vol. 362, pp. 200–203, 2004. [PubMed: 15158014]

[16]. Janssen J, “Advantages and disadvantages of GH/IGF-I combination treatment,” Reviews in endocrine and metabolic disorders, vol. 10, p. 157, 2009. [PubMed: 18604645]

[17]. Lee K, Silva EA, and Mooney DJ, “Growth factor delivery-based tissue engineering: general approaches and a review of recent developments,” Journal of the Royal Society Interface, vol. 8, pp. 153–170, 2011.

[18]. Brushart TM, Hoffman PN, Royall RM, Murinson BB, Witzel C, and Gordon T, “Electrical stimulation promotes motoneuron regeneration without increasing its speed or conditioning the neuron,” Journal of Neuroscience, vol. 22, pp. 6631–6638, 2002. [PubMed: 12151542]

[19]. Asensio-Pinilla E, Udina E, Jaramillo J, and Navarro X, “Electrical stimulation combined with exercise increase axonal regeneration after peripheral nerve injury,” Experimental neurology, vol. 219, pp. 258–265, 2009. [PubMed: 19500575]

[20]. Al-Majed AA, Brushart TM, and Gordon T, “Electrical stimulation accelerates and increases expression of BDNF and trkB mRNA in regenerating rat femoral motoneurons,” European Journal of Neuroscience, vol. 12, pp. 4381–4390, 2000. [PubMed: 11122348]

[21]. Kotwal A and Schmidt CE, “Electrical stimulation alters protein adsorption and nerve cell interactions with electrically conducting biomaterials,” Biomaterials, vol. 22, pp. 1055–1064, 2001. [PubMed: 11352099]

[22]. Lee J-W, Serna F, and Schmidt CE, “Carboxy-endcapped conductive polypyrrole: biomimetic conducting polymer for cell scaffolds and electrodes,” Langmuir, vol. 22, pp. 9816–9819, 2006. [PubMed: 17106966]

[23]. Haan N and Song B, “Therapeutic Application of Electric Fields in the Injured Nervous System,” Adv Wound Care (New Rochelle), vol. 3, pp. 156–165, 2 1 2014. [PubMed: 24761356]

[24]. Salmons S, Ashley Z, Sutherland H, Russold MF, Li F, and Jarvis JC, “Functional electrical stimulation of denervated muscles: basic issues,” Artificial organs, vol. 29, pp. 199–202, 2005. [PubMed: 15725216]

[25]. Guimard NK, Gomez N, and Schmidt CE, “Conducting polymers in biomedical engineering,” Progress in Polymer Science, vol. 32, pp. 876–921, 2007/8/01/ 2007.

[26]. Guo B, Glavas L, and Albertsson A-C, “Biodegradable and electrically conducting polymers for biomedical applications,” Progress in Polymer Science, vol. 38, pp. 1263–1286, 9// 2013.

[27]. Huang J, Zhang Y, Lu L, Hu X, and Luo Z, “Electrical stimulation accelerates nerve regeneration and functional recovery in delayed peripheral nerve injury in rats,” European Journal of Neuroscience, vol. 38, pp. 3691–3701, 2013. [PubMed: 24118464]

[28]. Huang L, Zhuang X, Hu J, Lang L, Zhang P, Wang Y, et al., “Synthesis of Biodegradable and Electroactive Multiblock Polylactide and Aniline Pentamer Copolymer for Tissue Engineering Applications,” Biomacromolecules, vol. 9, pp. 850–858, 2008/3/01 2008. [PubMed: 18260636]

[29]. Rivers TJ, Hudson TW, and Schmidt CE, “Synthesis of a Novel, Biodegradable Electrically Conducting Polymer for Biomedical Applications,” Advanced Functional Materials, vol. 12, pp. 33–37, 2002.

[30]. Balint R, Cassidy NJ, and Cartmell SH, “Conductive polymers: Towards a smart biomaterial for tissue engineering,” Acta Biomaterialia, vol. 10, pp. 2341–2353, 2014/6/01/ 2014. [PubMed: 24556448]

[31]. Langer R and Vacanti JP, “Tissue engineering,” Science, vol. 260, pp. 920–6, 5 14 1993. [PubMed: 8493529]

[32]. Croisier F and Jérôme C, “Chitosan-based biomaterials for tissue engineering,” European Polymer Journal, vol. 49, pp. 780–792, 2013/4/01/ 2013.

[33]. Sakai S, Hashimoto I, and Kawakami K, “Synthesis of an agarose-gelatin conjugate for use as a tissue engineering scaffold,” J Biosci Bioeng, vol. 103, pp. 22–6, 1 2007. [PubMed: 17298896]

[34]. Jacobsen PAL, Rafaelsen J, Nielsen JL, Juhl MV, Theilgaard N, and Larsen KL, “Distribution of grafted β-cyclodextrin in porous particles for bone tissue engineering,” Microporous and Mesoporous Materials, vol. 168, pp. 132–141, 2013/3/01/ 2013.

[35]. Müller FA, Müller L, Hofmann I, Greil P, Wenzel MM, and Staudenmaier R, “Cellulose-based scaffold materials for cartilage tissue engineering,” Biomaterials, vol. 27, pp. 3955–3963, 2006/7/01/ 2006. [PubMed: 16530823]

[36]. Duarte ARC, Mano JF, and Reis RL, “Preparation of starch-based scaffolds for tissue engineering by supercritical immersion precipitation,” The Journal of Supercritical Fluids, vol. 49, pp. 279–285, 2009/6/01/ 2009.

[37]. Wang M-D, Zhai P, Schreyer DJ, Zheng R-S, Sun X-D, Cui F-Z, et al., "Novel crosslinked alginate/hyaluronic acid hydrogels for nerve tissue engineering," Frontiers of Materials Science, vol. 7, pp. 269–284, 2013.

[38]. Wang X, He J, Wang Y, and Cui F-Z, "Hyaluronic acid-based scaffold for central neural tissue engineering," Interface Focus, vol. 2, pp. 278–291, 03/21. 01/06/received. 02/20/accepted 2012. [PubMed: 23741606]

[39]. Gumera C, Rauck B, and Wang Y, "Materials for central nervous system regeneration: bioactive cues," Journal of Materials Chemistry, vol. 21, pp. 7033–7051, 2011.

[40]. Hench LL and Polak JM, "Third-generation biomedical materials," Science, vol. 295, pp. 1014–7, 2 08 2002. [PubMed: 11834817]

[41]. James R, Nagarale RK, Sachan VK, Badalucco C, Bhattacharya PK, and Kumbar SG, "Synthesis and characterization of electrically conducting polymers for regenerative engineering applications: sulfonated ionic membranes," Polymers for Advanced Technologies, vol. 25, pp. 1439–1445, 2014.

[42]. Willand MP, Nguyen MA, Borschel GH, and Gordon T, "Electrical Stimulation to Promote Peripheral Nerve Regeneration," Neurorehabil Neural Repair, vol. 30, pp. 490–6, 6 2016. [PubMed: 26359343]

[43]. Nagarale RK, Gohil GS, and Shahi VK, "Recent developments on ion-exchange membranes and electro-membrane processes," Advances in Colloid and Interface Science, vol. 119, pp. 97–130, 2/28/ 2006. [PubMed: 16325751]

[44]. Jiang X, Lim SH, Mao H-Q, and Chew SY, "Current applications and future perspectives of artificial nerve conduits," Experimental neurology, vol. 223, pp. 86–101, 2010. [PubMed: 19769967]

[45]. Kumbar NRK S.G, "Biodegradable Conducting Polymeric Implants for Tissue Regeneration, Imaging and Drug Delivery Applications."

[46]. Kumbar HMD S.G., ""Composite Fibers and Matrices Thereof"," PCT Patent Application No. PCT/US16/15104, 2016.

[47]. James R, Kumbar SG, Laurencin CT, Balian G, and Chhabra AB, "Tendon tissue engineering: adipose-derived stem cell and GDF-5 mediated regeneration using electrospun matrix systems," Biomed Mater, vol. 6, p. 025011, 4 2011. [PubMed: 21436509]

[48]. James R, Toti US, Laurencin CT, and Kumbar SG, "Electrospun nanofibrous scaffolds for engineering soft connective tissues," Methods Mol Biol, vol. 726, pp. 243–58, 2011. [PubMed: 21424454]

[49]. Kumbar SG, James R, Nukavarapu SP, and Laurencin CT, "Electrospun nanofiber scaffolds: engineering soft tissues," Biomed Mater, vol. 3, p. 034002, 9 2008. [PubMed: 18689924]

[50]. Lee P, Tran K, Chang W, Fang YL, Zhou G, Junka R, et al., "Bioactive polymeric scaffolds for osteochondral tissue engineering: in vitro evaluation of the effect of culture media on bone marrow stromal cells," Polymers for Advanced Technologies, vol. 26, pp. 1476–1485, 2015.

[51]. Lee P, Tran K, Chang W, Shelke NB, Kumbar SG, and Yu X, "Influence of chondroitin sulfate and hyaluronic acid presence in nanofibers and its alignment on the bone marrow stromal cells: cartilage regeneration," Journal of biomedical nanotechnology, vol. 10, pp. 1469–1479, 2014. [PubMed: 25016647]

[52]. Yeo MG and Kim GH, "Preparation and characterization of 3D composite scaffolds based on rapid-prototyped PCL/β-TCP struts and electrospun PCL coated with collagen and HA for bone regeneration," Chemistry of Materials, vol. 24, pp. 903–913, 2011.

[53]. Balasubramanian P, Roether JA, Schubert DW, Beier JP, and Boccaccini AR, "Bi-layered porous constructs of PCL-coated 45S5 bioactive glass and electrospun collagen-PCL fibers," Journal of Porous Materials, vol. 22, pp. 1215–1226, 2015.

[54]. Lee P, Tran K, Zhou G, Bedi A, Shelke NB, Yu X, et al., "Guided differentiation of bone marrow stromal cells on co-cultured cartilage and bone scaffolds," Soft matter, vol. 11, pp. 7648–7655, 2015. [PubMed: 26292727]

[55]. Yu LM, Kazazian K, and Shoichet MS, "Peptide surface modification of methacrylamide chitosan for neural tissue engineering applications," J Biomed Mater Res A, vol. 82, pp. 243–55, 7 2007. [PubMed: 17295228]

[56]. Junka R, Valmikinathan CM, Kalyon DM, and Yu X, "Laminin Functionalized Biomimetic Nanofibers For Nerve Tissue Engineering," Journal of biomaterials and tissue engineering, vol. 3, pp. 494–502, 2013. [PubMed: 24083073]

[57]. Wei X-L, Wang Y, Long S, Bobeczko C, and Epstein A, "Synthesis and physical properties of highly sulfonated polyaniline," Journal of the American Chemical Society, vol. 118, pp. 2545–2555, 1996.

[58]. Bellot M, Galandrin S, Boularan C, Matthies HJ, Despas F, Denis C, et al., "Dual agonist occupancy of AT1-R-α2C-AR heterodimers results in atypical Gs-PKA signaling," Nature chemical biology, vol. 11, pp. 271–279, 2015/4// 2015. [PubMed: 25706338]

[59]. Shelke NB, Lee P, Anderson M, Mistry N, Nagarale RK, Ma X-M, et al., "Neural tissue engineering: nanofiber-hydrogel based composite scaffolds," Polymers for Advanced Technologies, vol. 27, pp. 42–51, 2016.

[60]. Kumbar SG and Harmon MD, "Composite fibers and matrices thereof," ed: Google Patents, 2018.

[61]. Shelke NB, Lee P, Anderson M, Mistry N, Nagarale RK, Ma XM, et al., "Neural tissue engineering: nanofiber-hydrogel based composite scaffolds," Polymers for Advanced Technologies, vol. 27, pp. 42–51, 2016.

[62]. Wei Y, Hudson S, Mayer J, and Kaplan D, "The crosslinking of chitosan fibers," Journal of Polymer Science Part A: Polymer Chemistry, vol. 30, pp. 2187–2193, 1992.

[63]. Chen A-H, Liu S-C, Chen C-Y, and Chen C-Y, "Comparative adsorption of Cu (II), Zn (II), and Pb (II) ions in aqueous solution on the crosslinked chitosan with epichlorohydrin," Journal of Hazardous materials, vol. 154, pp. 184–191, 2008. [PubMed: 18031930]

[64]. Shanahan M and Auriac Y, "Water absorption and leaching effects in cellulose diacetate," Polymer, vol. 39, pp. 1155–1164, 1998.

[65]. Nada AA, James R, Shelke NB, Harmon MD, Awad HM, Nagarale RK, et al., "A smart methodology to fabricate electrospun chitosan nanofiber matrices for regenerative engineering applications," Polymers for Advanced Technologies, vol. 25, pp. 507–515, 2014.

[66]. Guo J, Berbano SS, Guo H, Baker AL, Lanagan MT, and Randall CA, "Cold sintering process of composites: bridging the processing temperature gap of ceramic and polymer materials," Advanced Functional Materials, vol. 26, pp. 7115–7121, 2016.

[67]. Kumbar SG, Nukavarapu SP, James R, Nair LS, and Laurencin CT, "Electrospun poly (lactic acid-co-glycolic acid) scaffolds for skin tissue engineering," Biomaterials, vol. 29, pp. 4100–4107, 2008. [PubMed: 18639927]

[68]. Othman N, Piah M, Adzis Z, Ahmad H, and Ahmad N, "Simulation of voltage and electric-field distribution for contaminated glass insulator," in Research and Development (SCOReD), 2013 IEEE Student Conference on, 2013, pp. 116–120.

[69]. Yim EK, Pang SW, and Leong KW, "Synthetic nanostructures inducing differentiation of human mesenchymal stem cells into neuronal lineage," Experimental cell research, vol. 313, pp. 1820–1829, 2007. [PubMed: 17428465]

[70]. Yang Z and Wang KK, "Glial fibrillary acidic protein: from intermediate filament assembly and gliosis to neurobiomarker," Trends in neurosciences, vol. 38, pp. 364–374, 2015. [PubMed: 25975510]

[71]. Sensenbrenner M, Lucas M, and Deloulme J-C, "Expression of two neuronal markers, growth-associated protein 43 and neuron-specific enolase, in rat glial cells," Journal of molecular medicine, vol. 75, pp. 653–663, 1997. [PubMed: 9351704]

[72]. Soltani MH, Pichardo R, Song Z, Sangha N, Camacho F, Satyamoorthy K, et al., "Microtubule-associated protein 2, a marker of neuronal differentiation, induces mitotic defects, inhibits growth of melanoma cells, and predicts metastatic potential of cutaneous melanoma," The American journal of pathology, vol. 166, pp. 1841–1850, 2005. [PubMed: 15920168]

[73]. Yuan A, Rao MV, and Nixon RA, "Neurofilaments at a glance," ed: The Company of Biologists Ltd, 2012.

[74]. Li Y, Cao J, Chen M, Li J, Sun Y, Zhang Y, et al., "Abnormal neural progenitor cells differentiated from induced pluripotent stem cells partially mimicked development of TSC2 neurological abnormalities," Stem cell reports, vol. 8, pp. 883–893, 2017. [PubMed: 28344003]

[75]. Safaeijavan R, Soleimani M, Divsalar A, Eidi A, and Ardeshirylajimi A, "Biological behavior study of gelatin coated PCL nanofiberous electrospun scaffolds using fibroblasts," Journal of Paramedical Sciences, vol. 5, 2013.

[76]. Zavastin D, Cretescu I, Bezdadea M, Bourceanu M, Drăgan M, Lisa G, et al., "Preparation, characterization and applicability of cellulose acetate–polyurethane blend membrane in separation techniques," Colloids and Surfaces A: Physicochemical and Engineering Aspects, vol. 370, pp. 120–128, 2010.

[77]. Fernandes LL, Resende CX, Tavares DS, Soares GA, Castro LO, and Granjeiro JM, "Cytocompatibility of chitosan and collagen-chitosan scaffolds for tissue engineering," Polimeros, vol. 21, pp. 1–6, 2011.

[78]. Gregorio-Jauregui KM, Pineda MG, Rivera-Salinas JE, Hurtado G, Saade H, Martinez JL, et al., "One-step method for preparation of magnetic nanoparticles coated with chitosan," Journal of Nanomaterials, vol. 2012, p. 4, 2012.

[79]. Mendes LC, Falco APS, Pinho MS, and Marques PO, "Sulfonated polyaniline: influence of sulfonation routes on its thermal and structural characteristics," Materials Research, vol. 14, pp. 466–471, 2011.

[80]. Menczel JD and Prime RB, Thermal analysis of polymers: fundamentals and applications: John Wiley & Sons, 2014.

[81]. Plueddemann EP, Interfaces in Polymer Matrix Composites: Composite Materials vol. 6: Elsevier, 2016.

[82]. Anseth KS, Bowman CN, and Brannon-Peppas L, "Mechanical properties of hydrogels and their experimental determination," Biomaterials, vol. 17, pp. 1647–1657, 1996. [PubMed: 8866026]

[83]. Ge W, Ren C, Duan X, Geng D, Zhang C, Liu X, et al., "Differentiation of Mesenchymal Stem Cells into Neural Stem Cells Using Cerebrospinal Fluid," Cell biochemistry and biophysics, vol. 71, pp. 449–455, 2015. [PubMed: 25217067]

[84]. Gunther K, Appelt-Menzel A, Kwok CK, Walles H, and Metzger M, "Rapid Monolayer Neural Induction of induced Pluripotent Stem Cells Yields Stably Proliferating Neural Stem Cells," Journal of Stem Cell Research & Therapy, vol. 2016, 2016.

[85]. Cheng Y-C, Tsao C-W, Chiang M-Z, Chung C-A, Chien C-C, Hu W-W, et al., "Microfluidic platform for human placenta-derived multipotent stem cells culture and applied for enhanced neuronal differentiation," Microfluidics and Nanofluidics, vol. 18, pp. 587–598, 2015.

[86]. Kai D, Jiang S, Low ZW, and Loh XJ, "Engineering highly stretchable lignin-based electrospun nanofibers for potential biomedical applications," Journal of Materials Chemistry B, vol. 3, pp. 6194–6204, 2015.

[87]. Martínez-Campos E, Civantos A, Redondo JA, Guzmán R, Pérez-Perrino M, Gallardo A, et al., "Cell Adhesion and Proliferation on Sulfonated and Non-Modified Chitosan Films," AAPS PharmSciTech, pp. 1–9, 2016.

[88]. Bober P, Humpolíček P, Pacherník J, Stejskal J, and Lindfors T, "Conducting polyaniline based cell culture substrate for embryonic stem cells and embryoid bodies," RSC Advances, vol. 5, pp. 50328–50335, 2015.

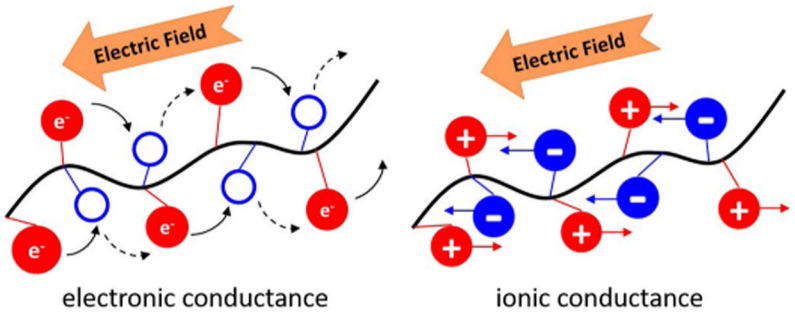

FIGURE 1:

Schematic representation illustrating the fundamental difference in conduction between electrically conducting and ionically conducting materials. Electronic conductance relies upon the movement of electrons and holes, whereas ionic conductance utilizes the opposite movement of positively and negatively charged ions.

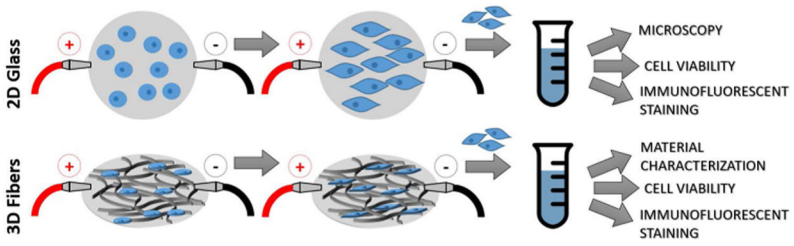

FIGURE 2:
Schematic of study design describing electrical stimulation cell studies on 2D ionically conducting-coated glass and 3D polymeric micro-nanofiber scaffolds.

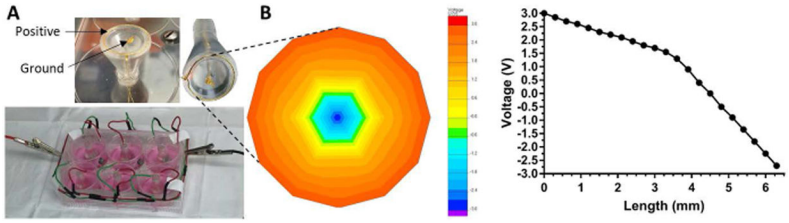

FIGURE 3:

(A) Custom-built electrical stimulation setup fitted for 6-well cell culture plate. A gold wire ring is designed as the positively-charged anode while a central gold wire is grounded, where each ring setup stimulates the contents of one well. (B) Voltage distribution map showing a prototype model conducting 3V with voltage decreasing in a concentric pattern towards the central ground.

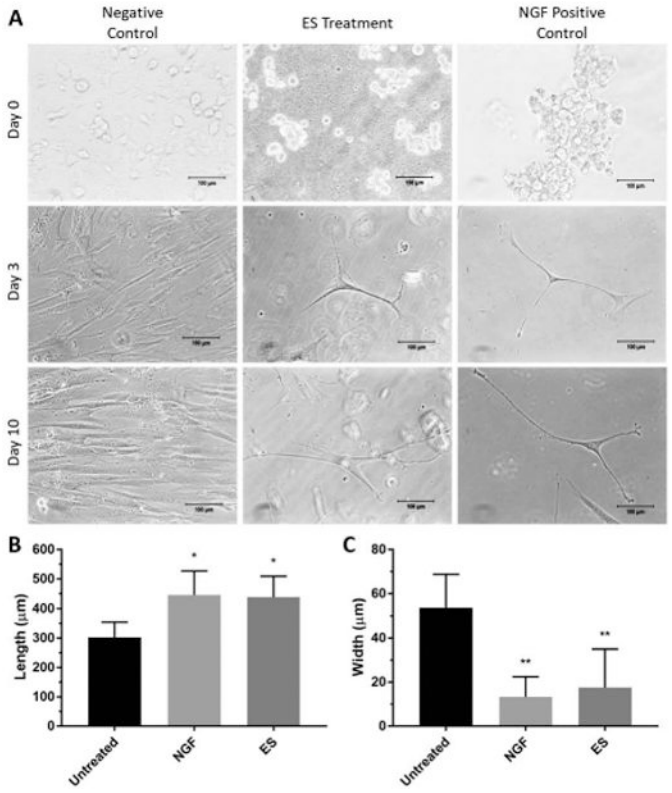

FIGURE 4:

(A) Phase-contrast microscopy of negative control (untreated), ES-, and NGF-treated (positive control) cell samples at various time points. Scale bar=100μm. ES and NGF samples show extension and branching typical of neuronal lineages, unlike untreated, negative control samples. (B) Cell length of untreated, NGF-treated, and ES cell samples at day 10 in culture where ES and NGF cells show greater cell length compared to untreated controls (*P<0.1). (C) Cell width of untreated (negative control), NGF-treated, and ES cell samples at day 10 in culture, where ES and NGF cells show statistically smaller width than untreated (negative control) samples (**P<0.05). Dimension measurements taken using an average of 100 cells.

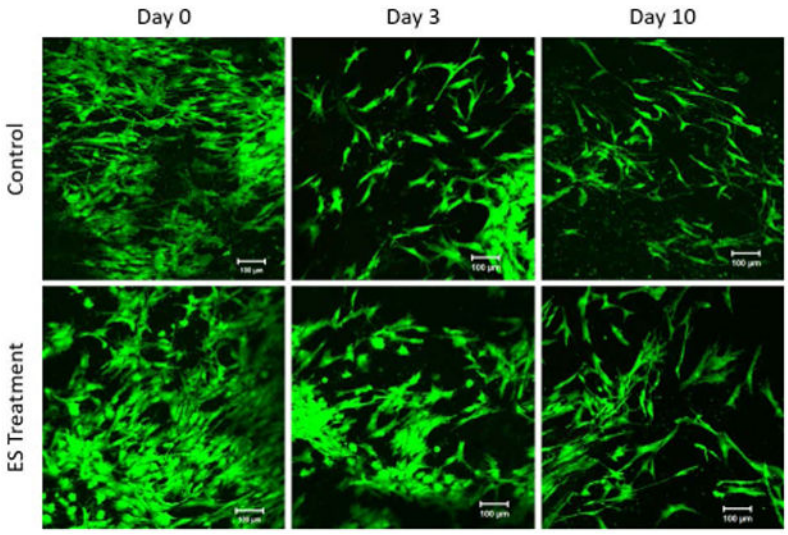

FIGURE 5:

LIVE/DEAD™ staining for cell viability of hMSCs seeded on CHT+SPANI coated glass coverslips treated with ES. Both ES and control (untreated) groups show similar cell viability indicating no differences in cell adhesion and/or viability as a result of applies ES. Morphological changes can be seen in day 10 ES-treated cells, having more profound protrusions, extensions, and branching.

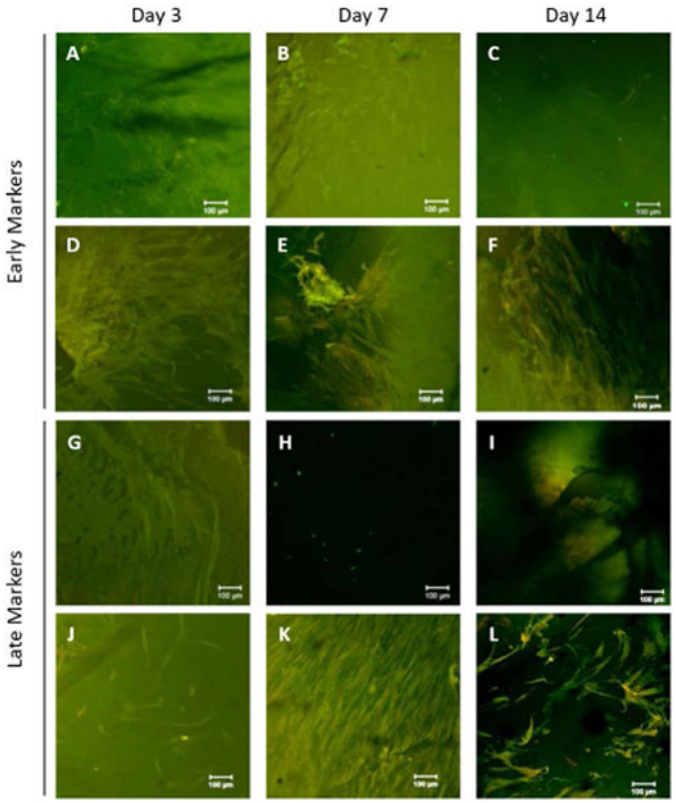

FIGURE 6:

Immunofluorescent staining of hMSCs seeded on CHT+SPANI coated glass coverslips treated with ES at day 3, 7, and 14. (A-C) Untreated control cells stained for GFAP (green) and NSE (red). (D-F) ES-treated cells stained for GFAP (green) and NSE (red). (G-I) Untreated control cells stained for B3TUB (green) and MAP2 (red). (J-L) ES-treated cells stained for B3TUB (green) and MAP2 (red).

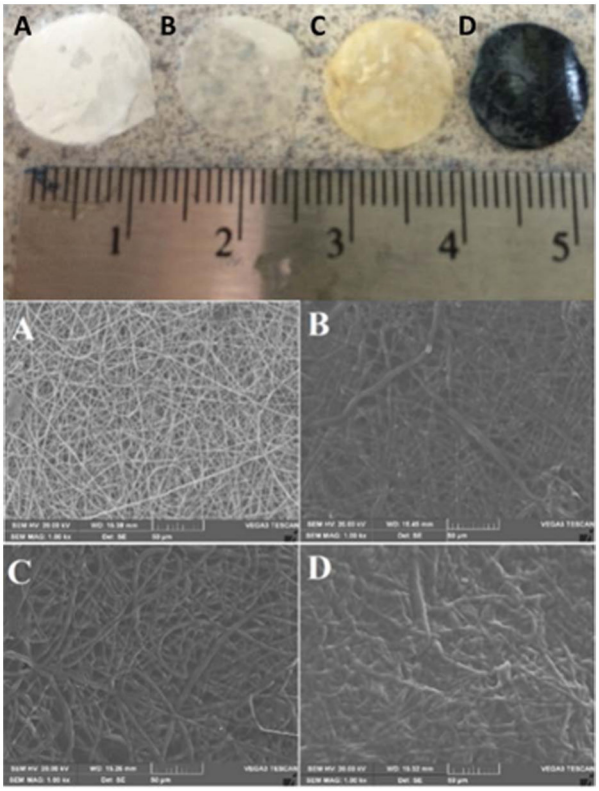

FIGURE 7:

Visual representation and size of circular scaffolds used for testing where (A) PCL/CA, (B) PCL/CA+CHT, (C) PCL/CA+CHT/LS, and (D) PCL/CA+CHT/SPANI. SEM images show the interconnected porous structure of micro-nanofibers of the aforementioned polymer composites, respectively. Hydrogel coatings can be seen in scaffolds B, C, and D due to the addition of CHT, CHT/LS, and CHT/SPANI, respectively.

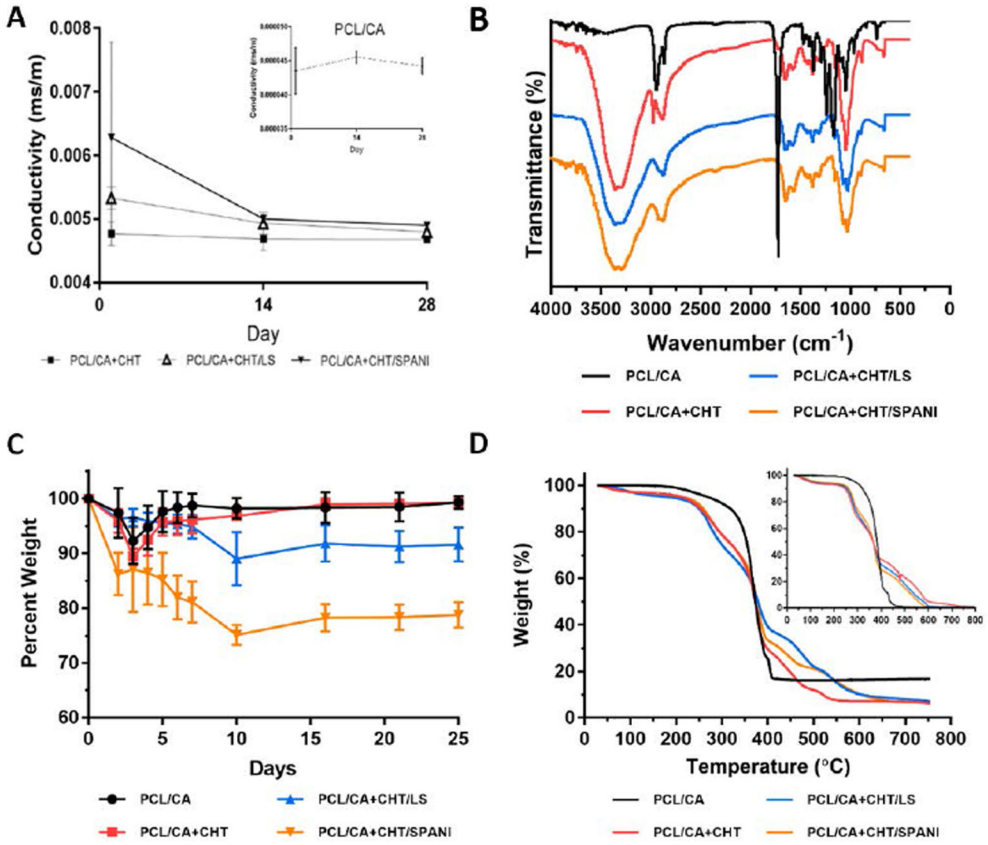

FIGURE 8:

(A) Conductivity studies of all four scaffold groups across 28 days showed a decrease of conductivity in PBS, eventually stabilizing after 28 days. (B) FTIR spectra of all four scaffold groups depicting key functional groups. (C) Weight loss studies of PCL/CA, PCL/CA+CHT, PCL/CA+CHT/LS, and PCL/CA+CHT/SPANI (D) TGA analysis of PCL/CA, PCL/CA+CHT, PCL/CA+CHT/LS, and PCL/CA+CHT/SPANI at week 4 (inset shows TGA at week 0).

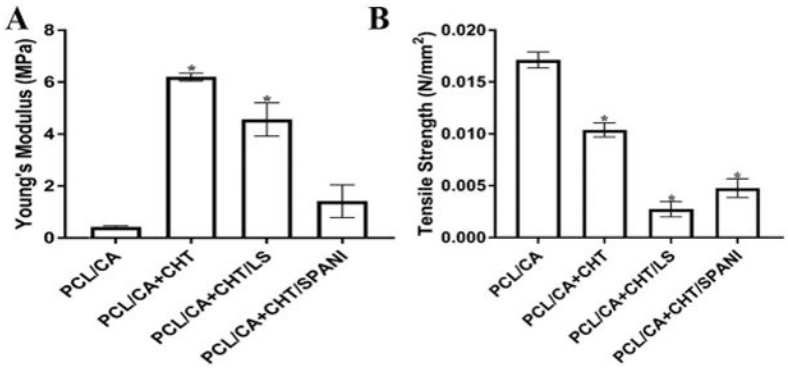

FIGURE 9:

(A) Young's modulus of PCL/CA, PCL/CA+CHT, PCL/CA+CHT/LS, and PCL/CA+CHT/SPANI (B) Tensile strength of PCL/CA, PCL/CA+CHT, PCL/ CA+CHT/LS, and PCL/CA +CHT/SPANI.

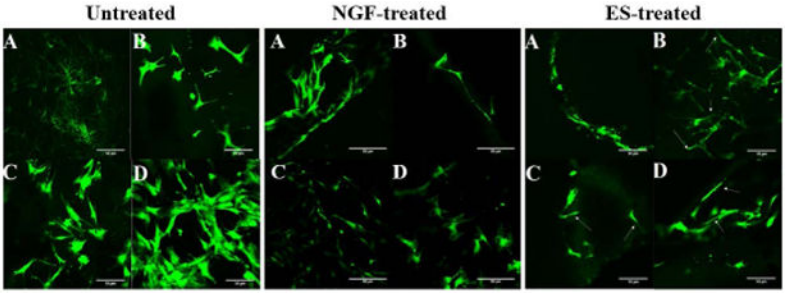

FIGURE 10:

LIVE/DEAD™ staining for cell viability of hMSCs on composite matrices for untreated (left), NGF-treated positive control (center), and ES-treated samples (right). Polymer compositions in all figures as follows: (A) PCL/CA, (B) PCL/CA+CHT, (C) PCL/ CA +CHT/LS and (D) PCL/CA+CHT/SPANI.

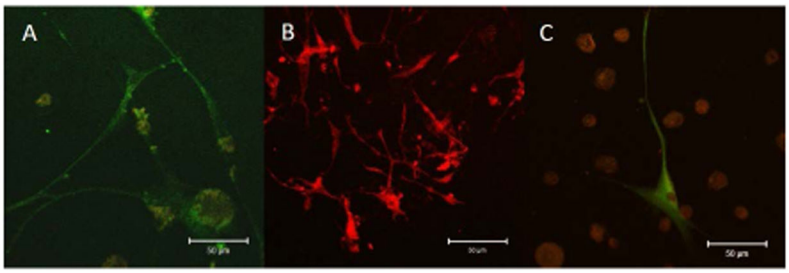

FIGURE 11:

Preliminary immunofluorescent staining of hMSCs on sulfonated polymers following 14-day ES showing staining for (A) B3-Tubulin (green), (B) MAP2 (red), and (C) Nestin (green). Scale bar=50μm.